machines

MDPI

Article

Inverse Kinematics and Statics-Based Motion Planning of a 7-DoF Transporter for DEMO-Type Breeding Blankets

Hjalte Durocher [1], Christian Bachmann [2], Rocco Mozzillo [3], Günter Janeschitz [4] and Xuping Zhang [1,*]

[1] Department of Mechanical and Production Engineering, Aarhus University, 8200 Aarhus N, Denmark; hdu@mpe.au.dk
[2] EUROfusion Consortium, FTD Department, 85748 Garching, Germany; christian.bachmann@euro-fusion.org
[3] CREATE, School of Engineering, Basilicata University, 85100 Potenza, Italy; rocco.mozzillo@unibas.it
[4] Max-Planck-Institut für Plasmaphysik, 85748 Garching, Germany; janeschgu@gmail.com
* Correspondence: xuzh@mpe.au.dk; Tel.: +45-41893167

Abstract

Future fusion power plants like DEMO must be remotely maintained for safety, including breeding blankets (BBs) weighing up to 180 t. The BB vertical transporter (BBVT), a crane-like redundant robot with 7 joints, has been previously designed for handling the five unique BB segments per sector. This includes grasping, preloading and collision-free spatial manipulation of BB segments in a space-constrained environment, necessitating advanced motion planning and real-time control. To achieve this, the challenge of obtaining accurate and performant inverse kinematic (IK) solutions for the redundant BBVT must be addressed. Therefore, a kinematic model is presented, and the redundant IK probelm is solved analytically for task-relevant cases, including derivation and analysis of the Jacobian. The model is verified by comparison with an MSC Adams model. Meanwhile, the analytical IK is found to be 53× to 84× faster than a gradient projection-based numerical solver in Matlab while providing multiple solutions. The IK and Jacobian are applied to create collision-free waypoints, verified in Matlab, for handling each BB segment while minimizing static joint loads in key configurations. A first-order estimate of the total BB handling time for a maintenance of nine days is calculated. These developments support the feasibility of the BBVT robot for the BB maintenance task in DEMO, and underpin future efforts in modelling dynamics and achieving real-time resilient control.

Keywords: kinematics; robotic manipulator; tokamak; breeding blanket; remote maintenance; motion planning

Check for updates

Received: 16 March 2026
Revised: 20 April 2026
Accepted: 21 April 2026
Published: 23 April 2026

Copyright: © 2026 by the authors. Licensee MDPI, Basel, Switzerland. This article is an open access article distributed under the terms and conditions of the Creative Commons Attribution (CC BY) license.

1. Introduction

Design work has been underway for the European demonstration fusion power plant EU-DEMO [1]. Several key technologies must be developed and tested before a future tokamak like DEMO can be successful; among them are tritium breeding blankets (BBs) [2] and remote maintenance tools [3]. Indeed, a primary task of the remote maintenance infrastructure at DEMO will be the safe and timely replacement of the blankets to ensure plant availability. In contrast to predecessors like JET [4] and ITER [5], a vertical BB maintenance architecture has been studied [6,7] and chosen for EU-DEMO for compatibility with smaller coils and reducing the amount of in- and ex-vessel maintenance operations [8,9]. Japanese DEMO [10], Korean K-DEMO [11] and Chinese CFETR [12] also pursue vertical BB maintenance schemes.

The nuclear fission industry has used a variety of robotic systems for such purposes as remote sensing and testing, decommissioning-related tasks such as disassembly and remediation, and maintenance and repair [13–15]. Mobile robots tend to be used for their reconnaissance and search-and-rescue capabilities in contaminated environments [16,17]. In the fusion context, the documented results from JET's dual-arm MASCOT robot continue to have high relevance [18].

For EU-DEMO, each tokamak sector is serviceable via an upper port and contains 5 BB segments: three outboard segments weighing up to 180 t and two inboard segments weighing up to 125 t. These are carried between the tokamak building and the active maintenance facility by a sealed cask on rails running above the buildings [19]. The crucial task of moving the BB segments between the vacuum vessel to the sealed cask via the upper port is to be carried out by the BB vertical transporter (BBVT), a special-purpose remote handling robot previously developed on a conceptual and mechanical level [20]. It is designed to be able to pick up each of the five BB segment shapes and manipulate them to or from the sealed cask while avoiding collisions within the space-constrained vacuum vessel and upper port. Its joint layout and gravity-locking gripper mechanism [21] minimize motion due to back-driving of joints in case of power loss.

With little simplification, the BBVT can be analyzed as a robotic manipulator with seven serial kinematic joints, as summarized in Figure 1a. In order to investigate in detail the BBVT's suitability for the BB maintenance task, two necessary prerequisites are the development of a kinematic model and a specific plan of desired spatial BB segment motions based on support disengagement [22] and collision avoidance. The existence of valid BBVT joint configurations corresponding to the handling motions, i.e., the existence of valid inverse kinematic (IK) solutions, should be confirmed. It is well-known that the solution of the IK problem for redundant manipulators, also known as redundancy resolution, is especially challenging. A host of general-purpose numerical algorithms are described in the literature, but analytical solutions are generally preferred in terms of accuracy [23]. As such, this work develops a kinematic BBVT model, finds task-relevant analytical IK solutions, and develops a detailed collision-free motion plan for BB segment removal. The motion plan and kinematic model are useful cornerstones for the further study of BB maintenance, for example, building towards trajectory generation, dynamic modelling, and the development of robust control strategies for a nuclear environment with gamma radiation and heating [24].

This work contains four sections. In Section 2, a kinematic model of the BBVT is presented and verified by comparison to a numerical model; analytical inverse kinematic algorithms are developed and their performance compared with numerical solvers, and the Jacobian matrix is derived. In Section 3, the inverse kinematics and Jacobian are used to develop detailed collision-free waypoints for the removal of each BB segment as well as to calculate and minimize static joint loads. Finally, in Section 4, the contributions and future work are discussed.

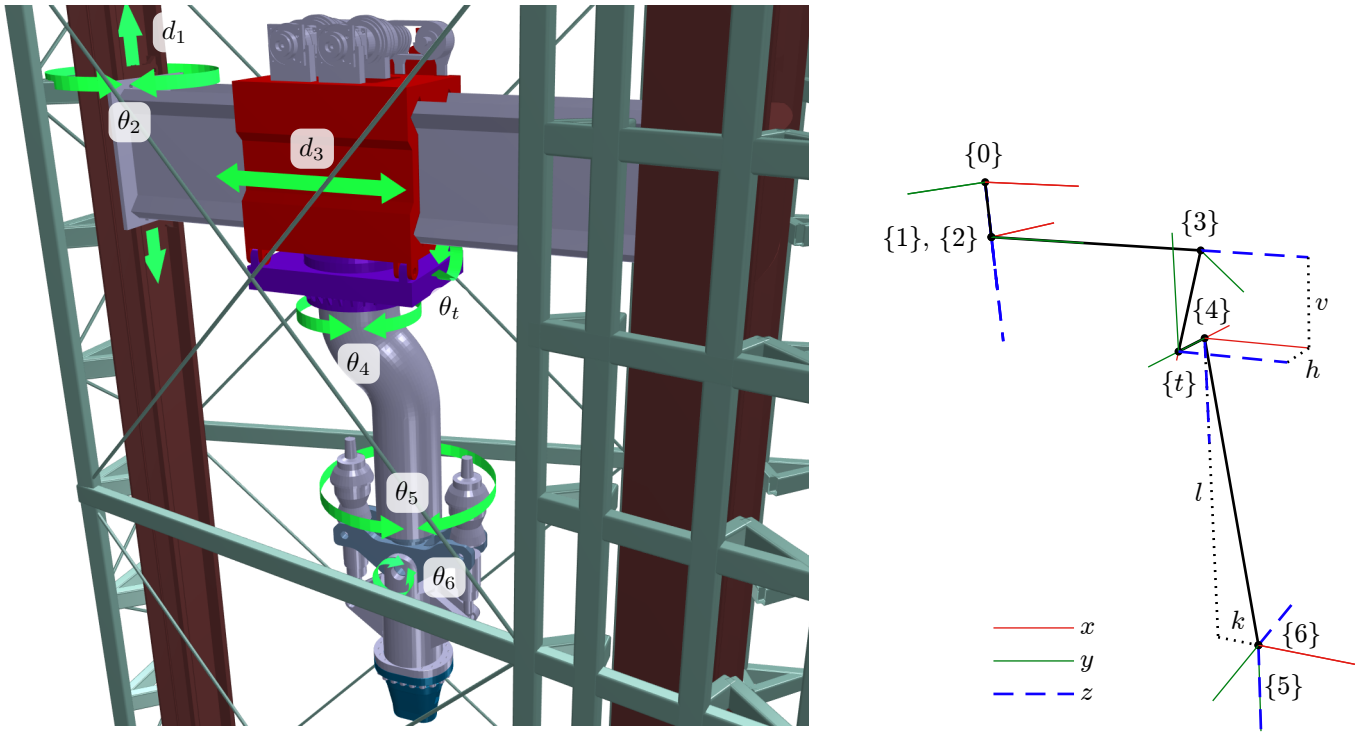

(**a**) Visualization of the BBVT's 7 joints. Green arrows illustrate the degree of freedom permitted by each joint.

(**b**) Link reference frames.

Figure 1. Overview of the BBVT's joints and links. The link reference frames are assigned and named according to the modified Denavit-Hartenberg convention of Craig [25], in which link frames $\{i-1\}$ and $\{i\}$ are connected by joint i.

2. Kinematics of the BB Vertical Transporter

The BBVT's task involves grasping, preloading and spatial manipulation of each BB segment. Rotations around the vertical and toroidal axes are required in order to avoid collisions while removing or replacing the segments. It is also practical to be able to make small adjustments to the orientation of the gripper around the radial axis for alignment of the gripper during grasping. In addition, torques must be applied by the gripper about toroidal and radial axes during preloading, whereby the weight of the grasped BB segment is carefully transferred to the BBVT without damaging mechanical supports [26,27]. For these reasons, the BBVT has been designed with a kinematic structure allowing full spatial motion of the end effector. The BBVT's 7 joints are visualized in Figure 1a and summarized in Table 1. The main kinematic simplification of the model lies in consolidating the three parallel elevator rigid chains (one inboard and two outboard) into a singular prismatic joint (d_1) located at the inboard.

Table 1. Summary of the BBVT's joints and modified D–H parameters. The fixed location of the gripper tool center point (TCP) frame is also given.

Name	i	Type	Variable	Limits	α_{i-1}	a_{i-1}	d_i	θ_i
Elevator	1	Prismatic	d_1	0 m to ∼30 m	0	0	d_1	$-90°$
Inboard hinge	2	Revolute	θ_2	$\pm 8.12°$	$-90°$	0	0	θ_2
Radial rail	3	Prismatic	d_3	0.93 m to 4.715 m	0	0	d_3	$-\arctan h/v - 90°$
Trolley tilting	t	Revolute	θ_t	$\pm 0.8°$	0	$\sqrt{h^2+v^2}$	0	$\theta_t + \arctan h/v + 90°$
Upper trunk	4	Revolute	θ_4	$\pm 180°$	$90°$	h	0	$\theta_4 + 90°$
Lower trunk	5	Revolute	θ_5	$\pm 180°$	0	k	l	θ_5
Gripper tilting	6	Revolute	θ_6	$\pm 8°$	$90°$	0	0	θ_6
Gripper TCP	G	Fixed	-	-	$-90°$	0	l_G	0

With its 7 joints, the BBVT is kinematically redundant with respect to its spatial (6-DoF) task. As the joint variables outnumber the task variables, the inverse kinematic problem is underdetermined for redundant manipulators. Many methods of tackling this redundancy resolution problem have been explored in the literature. The classic approach is to use the Moore–Penrose pseudoinverse of the non-square Jacobian matrix for a given joint configuration to iteratively converge to a least-squares solution at the velocity level [28]. A variety of enhancements to this method have been made, such as filters that improve the condition number near singularities [29] and techniques such as Jacobian weighting [30], gradient projection [31] and task augmentation [32] that control the optimization subtasks through modifying the Jacobian. Such techniques have successfully been applied to a wide variety of robots, including heavy-duty redundant manipulators used for nuclear decommissioning tasks [33]. In recent years, the formulation of redundancy resolution as a quadratic programming problem that can be efficiently solved using recurrent neural networks has gained traction [34]. Some researchers have also obtained analytical position-level IK solutions for specific 7-DoF manipulators by parameterizing the joint variables considering the self-motion of the mechanism [35–37].

Accurate motion planning and control of the BBVT will be bolstered if relevant analytical IK solutions can be obtained. However, such analytical solutions are challenging to find for redundant mechanisms like 7-DoF robotic arms. The most straightforward approach is to define a number of additional constraint equations equal to the difference in the number of variables. It happens that one of the BBVT joints, the trolley titling joint (joint variable θ_t), is meant to be immobile throughout the majority of the BB handling task, introducing a natural constraint that can be used to find relevant IK solutions for most purposes. Indeed, under some simplifying assumptions such as perfect rigidity of the BB and BBVT, θ_t will be 0 for the whole task, albeit still being used to apply large torques for preloading.

2.1. Forward Kinematics

The reference frame of the base link, link 0, lies on the rotational axis of the inboard hinge, at an arbitrary height in the cask such that the "home" position of the BBVT is near to the roof of the cask. This initial height can be easily adjusted with minimal impact on the kinematic results. The base link represents a common global frame for the docked cask, upper port and vacuum vessel sector, and therefore also functions as a global frame for the BBVT's operations. The axes of the global reference frame are consistent with the established convention for tokamaks, such that x_0 is the radial axis, y_0 is the toroidal axis, and z_0 is the poloidal axis.

The reference frames for links are attached according to the modified Denavit–Hartenberg (D-H) convention [25]. The D-H parameters for the BBVT are given in Table 1, with some key dimensional constants summarized in Table 2.

The D-H parameters can be used to calculate the homogeneous transformation matrices between links $i-1$ and i from the base to the outermost link, which can then be multiplied together to get the total transform:

$$ {}^{0}_{6}\boldsymbol{T} = {}^{0}_{1}\boldsymbol{T}\,{}^{1}_{2}\boldsymbol{T}\,{}^{2}_{3}\boldsymbol{T}\,{}^{3}_{t}\boldsymbol{T}\,{}^{t}_{4}\boldsymbol{T}\,{}^{4}_{5}\boldsymbol{T}\,{}^{5}_{6}\boldsymbol{T} = \begin{bmatrix} r_{11} & r_{12} & r_{13} & p_x \\ r_{21} & r_{22} & r_{23} & p_y \\ r_{31} & r_{32} & r_{33} & p_z \\ 0 & 0 & 0 & 1 \end{bmatrix}, \tag{1} $$

where

$$ r_{11} = \mathrm{s}_2\,\mathrm{s}_6\,\mathrm{s}_t + \mathrm{c}_2\,\mathrm{c}_4\,\mathrm{c}_5\,\mathrm{c}_6 - \mathrm{c}_2\,\mathrm{s}_4\,\mathrm{s}_5\,\mathrm{c}_6 - \mathrm{s}_2\,\mathrm{c}_4\,\mathrm{s}_5\,\mathrm{c}_6\,\mathrm{c}_t - \mathrm{s}_2\,\mathrm{s}_4\,\mathrm{c}_5\,\mathrm{c}_6\,\mathrm{c}_t \tag{2} $$

$$ r_{21} = -\,\mathrm{c}_2\,\mathrm{s}_6\,\mathrm{s}_t + \mathrm{s}_2\,\mathrm{c}_4\,\mathrm{c}_5\,\mathrm{c}_6 - \mathrm{s}_2\,\mathrm{s}_4\,\mathrm{s}_5\,\mathrm{c}_6 + \mathrm{c}_2\,\mathrm{c}_4\,\mathrm{s}_5\,\mathrm{c}_6\,\mathrm{c}_t + \mathrm{c}_2\,\mathrm{s}_4\,\mathrm{c}_5\,\mathrm{c}_6\,\mathrm{c}_t \tag{3} $$

$$r_{31} = s_6\, c_t + c_4\, s_5\, c_6\, s_t + s_4\, c_5\, c_6\, s_t \tag{4}$$

$$r_{12} = s_2\, c_6\, s_t + c_2\, s_4\, s_5\, s_6 - c_2\, c_4\, c_5\, s_6 + s_2\, s_4\, c_5\, s_6\, c_t + s_2\, c_4\, s_5\, s_6\, c_t \tag{5}$$

$$r_{22} = -\, c_2\, c_6\, s_t + s_2\, s_4\, s_5\, s_6 - s_2\, c_4\, c_5\, s_6 - c_2\, s_4\, c_5\, s_6\, c_t - c_2\, c_4\, s_5\, s_6\, c_t \tag{6}$$

$$r_{32} = c_6\, c_t - c_4\, s_5\, s_6\, s_t - s_4\, c_5\, s_6\, s_t \tag{7}$$

$$r_{13} = c_2\, c_4\, s_5 + c_2\, s_4\, c_5 + s_2\, c_4\, c_5\, c_t - s_2\, s_4\, s_5\, c_t \tag{8}$$

$$r_{23} = s_2\, c_4\, s_5 + s_2\, s_4\, c_5 - c_2\, c_4\, c_5\, c_t + c_2\, s_4\, s_5\, c_t \tag{9}$$

$$r_{33} = s_4\, s_5\, s_t - c_4\, c_5\, s_t \tag{10}$$

$$p_x = k(c_2\, c_4 - s_2\, s_4\, c_t) + c_2\, d_3 - h\, s_2(1 - c_t) + l\, s_2\, s_t \tag{11}$$

$$p_y = k(s_2\, c_4 + c_2\, s_4\, c_t) + s_2\, d_3 + h\, c_2(1 - c_t) - l\, c_2\, s_t \tag{12}$$

$$p_z = d_1 + l\, c_t - (h - k\, s_4)\, s_t + v. \tag{13}$$

In (2)–(13), the compact notation $s_x = \sin(\theta_x)$ and $c_x = \cos(\theta_x)$ has been used.

Table 2. Key dimensions of the BBVT.

Description	Symbol	Value
Horizontal distance from link 3 to link t	h	0.488 m
Vertical distance from link 3 to link t	v	0.78 m
Trunk length	l	3.05225 m
Trunk kink distance	k	0.438 m
Gripper length	l_G	1.845 m

Verification

A kinematic model of the BBVT has been implemented in the MSC Adams 2023.2 simulation software and is used to verify the analytical model. This is done by inputting a test trajectory to the two models and comparing the resulting predicted gripper TCP path. The test trajectory consists of the sinusoidal driving of every joint at different frequencies (Figure 2a). With an overall RMSE of 2.3527×10^{-7} m, the results, shown in Figure 2b–e, indicate agreement between the gripper path in ADAMS and the analytical model. In addition, a kinematically accurate down-scaled prototype of the robot has been built.

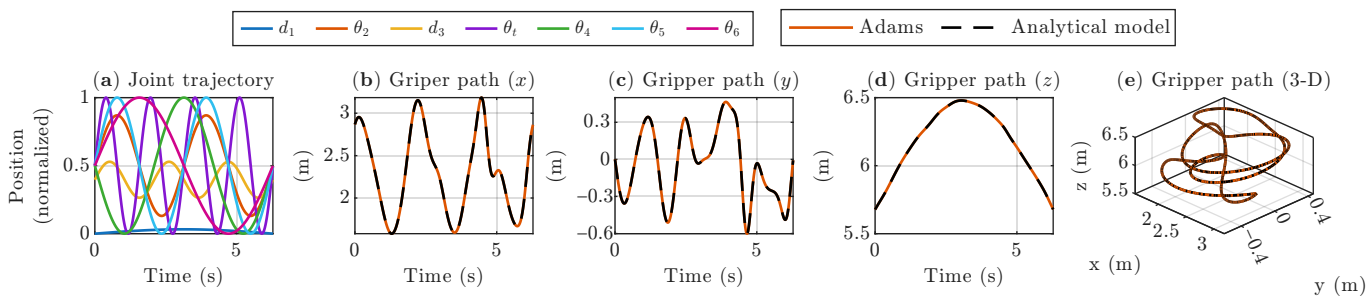

Figure 2. Comparison of the predicted gripper TCP path (**b**–**e**) between the ADAMS model and the analytical forward kinematic model for a test trajectory involving every joint (**a**).

2.2. Inverse Kinematics

For control, and when developing waypoints, it is useful to calculate one or more valid joint configurations that will result in the BBVT outermost link having a desired spatial pose relative to the base, defined by the transform ${}^0_6\boldsymbol{T}$. While iterative numerical methods can readily be applied to solve this inverse kinematic problem, an analytical solution can improve accuracy and give greater insight into the kinematics of the mechanism. With 7 unknown joint variables, the inverse kinematic problem can only be solved analytically for the BBVT if at least one joint variable is known beforehand.

Incidentally, the trolley tilting joint is only designed to be active for a limited subset of the BB handling task, namely engagement and preloading. Beforehand, while approaching the target BB segment, θ_t will be set to 0. Afterward, while manipulating the BB segment, it will be locked to a small angle that is naturally reached at the end of preloading. Under the simplifying assumptions:

(a) The BB segments are perfectly positioned with no radial tilt;
(b) There are no gaps between the gripper and interface when engaged;
(c) The BB segments and the BBVT links are perfectly rigid;
(d) BBVT joints are perfectly rigid with no backlash.

Then, $\theta_t = 0$ for the entire task. For simplicity, these assumptions are used later in this work when developing ideal waypoints for the removal task and calculating static loads. The inverse kinematics are here solved for the general case of $\theta_t \neq 0$ as well as the special case $\theta_t = 0$. In the real scenario, the constant but unknown value of θ_t during BB manipulation will vary depending on highly uncertain variables such as misalignments, gaps, and deflections.

A procedure for analytically calculating the values of the unknown joint variables of the BBVT given a target position of the outermost link in the form of a homogeneous transformation matrix ${}^0_6\boldsymbol{T}$ like Equation (1), and assuming that θ_t is known, is presented in the following subsections.

2.2.1. Joint 2

Equation (10) is used as a starting point to calculate $\cos(\theta_4 + \theta_5)$, using the sum of angles formula:

$$\begin{aligned} r_{33} &= \mathrm{s}_4\,\mathrm{s}_5\,\mathrm{s}_t - \mathrm{c}_4\,\mathrm{c}_5\,\mathrm{s}_t \\ &= -\,\mathrm{c}_{45}\,\mathrm{s}_t \end{aligned} \tag{14}$$

$$\mathrm{c}_{45} = -\frac{r_{33}}{\mathrm{s}_t} \tag{15}$$

$\sin(\theta_4 + \theta_5)$ then takes on two possible values:

$$\mathrm{s}_{45} = \pm\sqrt{1 - \mathrm{c}_{45}^2} \tag{16}$$

Next, the sum of angles formulae are used on Equations (8) and (9), and the resulting system of equations is solved for θ_2, with two solutions possible depending on the sign of s_{45}:

$$r_{13} = \mathrm{c}_2 + \mathrm{s}_2\,\mathrm{c}_t\,\mathrm{c}_{45} \tag{17}$$

$$r_{23} = \mathrm{s}_2\,\mathrm{s}_{45} - \mathrm{c}_2\,\mathrm{c}_t\,\mathrm{c}_{45} \tag{18}$$

$$\theta_2 = \mathrm{atan2}(r_{13}\,\mathrm{c}_t\,\mathrm{c}_{45} + \mathrm{s}_{45}\,r_{23},\ r_{13}\,\mathrm{s}_{45} - \mathrm{c}_t\,\mathrm{c}_{45}\,r_{23}) \tag{19}$$

2.2.2. Joint 4

Equations (11) and (12) can be set equal by solving for d_3, giving

$$\mathrm{c}_2\big(p_y - k(\mathrm{s}_2\,\mathrm{c}_4 + \mathrm{c}_2\,\mathrm{s}_4\,\mathrm{c}_t) + g\,\mathrm{c}_2\big) = \mathrm{s}_2(p_x - k(\mathrm{c}_2\,\mathrm{c}_4 - \mathrm{s}_2\,\mathrm{s}_4\,\mathrm{c}_t) + g\,\mathrm{s}_2) \tag{20}$$

where the convenient constant g has been defined:

$$g \equiv l\,\mathrm{s}_t - h(1 - \mathrm{c}_t) \tag{21}$$

Equation (20) simplifies to:

$$g\left(\mathrm{s}_2^2 + \mathrm{c}_2^2\right) + p_y\,\mathrm{c}_2 - p_x\,\mathrm{s}_2 = k\,\mathrm{c}_4(-\mathrm{s}_2\,\mathrm{c}_2 + \mathrm{s}_2\,\mathrm{c}_2) + k\,\mathrm{s}_4\left(\mathrm{c}_t\left(\mathrm{s}_2^2 + \mathrm{c}_2^2\right)\right) \tag{22}$$

$$g + p_y\, c_2 - p_x\, s_2 = k\, s_4\, c_t \tag{23}$$

which can be solved for s_4:

$$s_4 = \frac{g + p_y\, c_2 - p_x\, s_2}{k\, c_t} \tag{24}$$

Recalling the two solutions for θ_2, four solutions are then available for θ_4:

$$c_4 = \pm\sqrt{1 - s_4^2} \tag{25}$$

$$\theta_4 = \text{atan2}(s_4,\, c_4) \tag{26}$$

2.2.3. Joint 5

Recalling the availability of two solutions each for s_{45} and θ_4, four solutions are found for θ_5:

$$\theta_5 = \text{atan2}(s_{45},\, c_{45}) - \theta_4 \tag{27}$$

2.2.4. Joint 3

Recalling the availability of two solutions each for θ_2 and θ_4, Equation (11) can be used to obtain four solutions for d_3:

$$d_3 = \frac{p_x}{c_2} - k(c_4 - t_2\, s_4\, c_t) + h t_2 (1 - c_t) - l t_2\, s_t \tag{28}$$

where $t_2 \equiv \tan\theta_2$.

2.2.5. Joint 1

Using Equation (13) and the solution for s_4 from Equation (24), d_1 can be obtained:

$$d_1 = p_z - l\, c_t + s_t(h - k\, s_4) - v \tag{29}$$

where there are two solutions because s_4 depends on θ_2, which depends on s_{45}.

2.2.6. Joint 6

Equations (4) and (7) can be rewritten using the sum of angles formulae. The resulting system of equations can then be solved for θ_6, resulting in two solutions corresponding to those of s_{45} in Equation (16):

$$r_{31} = s_6\, c_t + c_4\, s_5\, c_6\, s_t + s_4\, c_5\, c_6\, s_t = s_6\, c_t + c_6\, s_t\, s_{45} \tag{30}$$

$$r_{32} = c_6\, c_t - c_4\, s_5\, s_6\, s_t - s_4\, c_5\, s_6\, s_t = c_6\, c_t - s_6\, s_t\, s_{45} \tag{31}$$

$$\theta_6 = \text{atan2}(r_{31}\, c_t - r_{32}\, s_t\, s_{45},\, r_{32}\, c_t + r_{31}\, s_t\, s_{45}) \tag{32}$$

2.2.7. Summary, Multiple Solutions, and Unknown θ_t

To summarize the above developments, Equation (16) results in two solutions for s_{45}, each of which is associated with a unique solution for d_1, θ_2, and θ_6. Further, each solution for s_{45} is associated with a unique pair of solutions for c_4, leading to four solutions each for the joint variables d_3, θ_4 and θ_5, and four overall solutions to the inverse kinematic problem where θ_t is known. An example pose with all four IK solutions overlaid is depicted in Figure 3b. It should be noted that the existence and uniqueness of solutions are not guaranteed. For example, it is evident that if either $\theta_4 + \theta_5 = \frac{\pi}{2} \pm n\pi$ or $\theta_4 = 0 \pm n\pi$, at most two solutions can be unique.

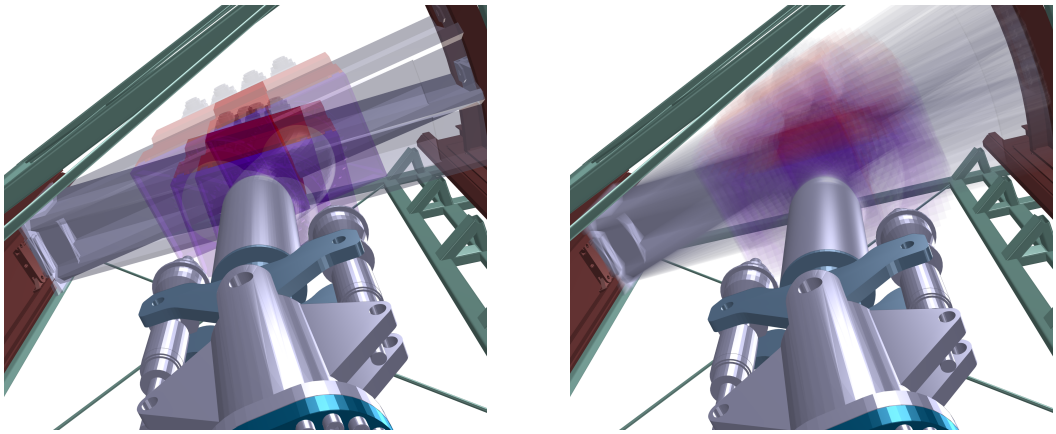

(**a**) (**b**)

Figure 3. Visualization of (**a**) all 4 IK solutions for a pose with $\theta_t = -0.8°$ and (**b**) some of the continuous range of IK solutions for a pose with with $\theta_t = 0$ (30 shown).

In the case when θ_t is unknown, a similar approach can be taken, though it requires predefining the sum $\theta_4 + \theta_5$ (not the individual angles). Then, Equations (15) and (16) can be modified to instead solve for θ_t (with two solutions), and the procedure followed from there. For preloading, it may be more intuitive to define θ_2 together with $\theta_4 + \theta_5$ in order to fully specify the desired tilting axis orientations, as will be described in Section 3.2.1.

2.3. A Special Inverse Kinematic Case

The procedure presented in Section 2.2 fails in the special case of $\theta_t = 0$, in which Equation (2) through (13) reduce to

$$r_{11} = c_2\,c_4\,c_5\,c_6 - c_2\,s_4\,s_5\,c_6 - s_2\,c_4\,s_5\,c_6 - s_2\,s_4\,c_5\,c_6 \tag{33}$$
$$r_{21} = s_2\,c_4\,c_5\,c_6 - s_2\,s_4\,s_5\,c_6 + c_2\,c_4\,s_5\,c_6 + c_2\,s_4\,c_5\,c_6 \tag{34}$$
$$r_{31} = s_6 \tag{35}$$
$$r_{12} = c_2\,s_4\,s_5\,s_6 - c_2\,c_4\,c_5\,s_6 + s_2\,s_4\,c_5\,s_6 + s_2\,c_4\,s_5\,s_6 \tag{36}$$
$$r_{22} = s_2\,s_4\,s_5\,s_6 - s_2\,c_4\,c_5\,s_6 - c_2\,s_4\,c_5\,s_6 - c_2\,c_4\,s_5\,s_6 \tag{37}$$
$$r_{32} = c_6 \tag{38}$$
$$r_{13} = c_2\,c_4\,s_5 + c_2\,s_4\,c_5 + s_2\,c_4\,c_5 - s_2\,s_4\,s_5 \tag{39}$$
$$r_{23} = s_2\,c_4\,s_5 + s_2\,s_4\,c_5 - c_2\,c_4\,c_5 + c_2\,s_4\,s_5 \tag{40}$$
$$r_{33} = 0 \tag{41}$$
$$p_x = (c_2\,c_4 - s_2\,s_4)k + c_2\,d_3 \tag{42}$$
$$p_y = (s_2\,c_4 + c_2\,s_4)k + s_2\,d_3 \tag{43}$$
$$p_z = d_1 + l. \tag{44}$$

An algebraic approach to finding the constraints on the inverse kinematic solutions can still be undertaken. Equations (35), (38) and (44) give d_1 and θ_6 directly:

$$d_1 = p_z - l \tag{45}$$

and

$$\theta_6 = \text{atan2}(r_{31}, r_{32}). \tag{46}$$

Equations (42) and (43) can be rewritten as

$$p_{3x} \equiv d_3\, \mathrm{c}_2 = p_x + \cos\left(\theta_2 + \theta_4 + \pi\right)k \tag{47}$$

$$p_{3y} \equiv d_3\, \mathrm{s}_2 = p_y + \sin\left(\theta_2 + \theta_4 + \pi\right)k, \tag{48}$$

which is the parametric form of the equation of a circle with center $\left(p_x, p_y\right)$ and radius k, and p_{3x} and p_{3y} are the x- and y-coordinates of the trolley link (frame $\{3\}$).

Finally, Equations (39) and (40) can be expressed in the form

$$r_{13} = \sin\left(\theta_2 + \theta_4 + \theta_5\right) \tag{49}$$

$$-r_{23} = \cos\left(\theta_2 + \theta_4 + \theta_5\right), \tag{50}$$

which leads to a constraint on the sum of the three unknown joint angles:

$$\theta_2 + \theta_4 + \theta_5 = \mathrm{atan2}(r_{13}, -r_{23}). \tag{51}$$

Thus, the inverse kinematic solutions in the case where $\theta_t = 0$ are constrained by Equations (47), (48) and (51). The first two equations constrain the trolley x and y coordinates to lie on a circle centered on the target point, suggesting a convenient parameterization of θ_2 and d_3 using an angle parameter. The third equation constrains the sum of the vertical joint angles to ensure the correct orientation of the outermost link. As an example, Figure 3a depicts 30 overlaid inverse kinematic solutions for a pose where $\theta_t = 0$. The existence of infinite solutions means that the BBVT mechanism regains its redundant character in the case when θ_t is constrained to be 0, as opposed to $\theta_t \neq 0$. This will be made clear in the following subsection regarding the Jacobian matrix.

If either θ_5 or $\theta_2 + \theta_4$ is known, then a single inverse kinematic solution can be found based on the constraints. The same is true if d_3 and either θ_2 or θ_4 is known. If only θ_2, d_3 or θ_4 is known, then two valid solutions can be found. The joint variables d_1 and θ_6 take on single values for all solutions according to (45) and (46).

2.4. Jacobian

The Cartesian velocity of the outermost frame can be found by the propagation of velocity outwards from link to link (see Appendix A for details). Based on this, the analytical configuration-dependent 6×7 Jacobian matrix relating joint velocities and Cartesian end-effector velocities can be constructed. Although it is too large to reproduce here, the simplified case where $\theta_t = 0$ is:

$$
{}^{6}\boldsymbol{J}_{\theta_t=0} = \begin{bmatrix}
\mathrm{s}_6 & k\,\mathrm{s}_5\,\mathrm{c}_6 + d_3\,\mathrm{s}_{45}\,\mathrm{c}_6 & \mathrm{c}_{45}\,\mathrm{c}_6 & k\,\mathrm{s}_4\,\mathrm{s}_6 - h\,\mathrm{s}_6 - l\,\mathrm{s}_{45}\,\mathrm{c}_6 & k\,\mathrm{s}_5\,\mathrm{c}_6 & 0 & 0 \\
\mathrm{c}_6 & -k\,\mathrm{s}_5\,\mathrm{s}_6 - d_3\,\mathrm{s}_{45}\,\mathrm{s}_6 & -\mathrm{c}_{45}\,\mathrm{s}_6 & k\,\mathrm{c}_6\,\mathrm{s}_4 - h\,\mathrm{c}_6 + l\,\mathrm{s}_{45}\,\mathrm{s}_6 & -k\,\mathrm{s}_5\,\mathrm{s}_6 & 0 & 0 \\
0 & d_3\,\mathrm{c}_{45} - k\,\mathrm{c}_5 & \mathrm{s}_{45} & l\,\mathrm{c}_4\,\mathrm{c}_5 - l\,\mathrm{s}_4\,\mathrm{s}_5 & -k\,\mathrm{c}_5 & 0 & 0 \\
0 & \mathrm{s}_6 & 0 & \mathrm{c}_{45}\,\mathrm{c}_6 & \mathrm{s}_6 & \mathrm{s}_6 & 0 \\
0 & \mathrm{c}_6 & 0 & -\mathrm{c}_{45}\,\mathrm{s}_6 & \mathrm{c}_6 & \mathrm{c}_6 & 0 \\
0 & 0 & 0 & \mathrm{s}_{45} & 0 & 0 & 1
\end{bmatrix}. \tag{52}
$$

The form of the Jacobian in Equation (52) is useful to calculate the static joint loads $\boldsymbol{\tau} = \begin{bmatrix}\tau_1 & \tau_2 & \tau_3 & \tau_t & \tau_5 & \tau_6 & \tau_7\end{bmatrix}^\top$ at the joint configuration $\boldsymbol{\Theta}_{\theta_t=0}$ due to the external force $\boldsymbol{F}$ and moment $\boldsymbol{n}$ loads on the last link ${}^{6}\boldsymbol{\mathcal{F}}_6 = \begin{bmatrix}{}^{6}\boldsymbol{F}_6^\top & {}^{6}\boldsymbol{n}_6^\top\end{bmatrix}^\top$, based on the relationship

$$\boldsymbol{\tau} = \boldsymbol{J}(\boldsymbol{\Theta})^\top \boldsymbol{\mathcal{F}}. \tag{53}$$

When the trolley tilting joint is considered locked (immobile and incapable of producing torque), the fourth column should be omitted from Equation (52). The resulting 6×6 Jacobian is singular with $\mathbf{\Theta}_{\theta_t=0}$. When rotated to align with frame $\{5\}$, the fourth row becomes all zeros and can also be removed to recover a full-rank, non-square matrix. This reflects the reduction in both mechanism DoF and task-space DoF when θ_t is locked to 0, ensuring redundancy is maintained from the unlocked mechanism.

A singularity exists when $\theta_t = 0$ and $\theta_4 + \theta_5 = \frac{\pi}{2} \pm n\pi$. In such configurations, the two tilting joint axes (θ_t and θ_6) become parallel. This must be taken into account when performing calculations with the Jacobian, although the singularity is not likely to be approached during normal operation of the BBVT because the designed use-case of the two tilting joints is to supply perpendicular moments.

2.5. Comparison to Numerical Solvers

The IK algorithms for when $\theta_t \neq 0$ and $\theta_t = 0$, described in Section 2.2 and Section 2.3 respectively, are implemented in Matlab. Their performance is compared to three numerical inverse kinematics solvers available in Matlab Robotics Toolbox R2025b: `BFGS`, a gradient projection-based algorithm [38], `LM`, a damped pseudoinverse algorithm [39], and `fminconsqp`, a quadratic programming-based algorithm [40]. Although various constraints such as joint limits can be used with these solvers, none are used here in order to have a level comparison (for the analytical solvers, joint limits could be simply applied by filtering the solutions). Each method is applied to the same set of 1000 random valid transporter poses, with each solution timed using the `tic` and `toc` functions. For the numerical solvers, the home configuration is used as an initial guess, and the default solution tolerances and other solver options are used. The code is run on a laptop with an i7-1165G7 processor and 16 GB of memory.

The statistical summary of the results is given in Table 3. The analytical algorithms are $53\times$ to $84\times$ faster on average than the fastest numerical solver (`BFGS`) in the test. The other two numerical solvers perform worse, with less than 100% success rate and slower times. Also, whereas the numerical solvers always yield a single solution, the analytical algorithms give all four solutions when $\theta_t \neq 0$ or arbitrarily many (in the test case, 100) solutions when $\theta_t = 0$. On the other hand, the analytical algorithm always requires specifying θ_t in order function, while the numerical solvers can succeed when θ_t is unknown or unspecified. It is also likely that the solvers, especially `LM`, would perform better with more accurate initial guesses—however, a strength of the analytical solutions is the lack of need for such guesses.

Table 3. Comparison of the analytical IK algorithms to numerical IK solvers in Matlab, applied to a set of 1000 random valid poses. In the case where $\theta_t = 0$, the degree of freedom is removed from the BBVT kinematic model, leading to a slight improvement of the analytical solvers' performance.

Algorithm	$\theta_t \neq 0$			$\theta_t = 0$		
	Mean Time (ms)	**Succ. Rate**	**Num. Sols.**	**Mean Time (ms)**	**Succ. Rate**	**Num. Sols.**
Analytical	0.0863	100%	4	0.0284	100%	100
`BFGS`	4.55	100%	1	2.38	100%	1
`LM`	113	88.1%	1	115	96.7%	1
`fminconsqp`	9.17	96.1%	1	5.76	100%	1

3. Motion Planning

A closely linked problem to that of inverse kinematics is motion planning. Autonomous robots in unstructured environments particularly require algorithms that can generate appropriate motions between starting and goal poses subject to dynamic task-relevant constraints such as collision avoidance. Perhaps the most widespread approach is

the class of probabilistic sampling-based algorithms typified by rapidly-exploring rapid trees (RRT) [41]. Other approaches include artificial potential fields (APF) and evolutionary algorithms [42,43], and, increasingly, AI-based task and motion planning (TAMP) [44], potentially augmented by emerging technologies such as vision-language models (VLMs) [45]. While such planning algorithms will likely be useful to robustly handle mechanical and sensing uncertainties in the BB maintenance task, the ideal task environment is highly structured such that dynamic planning is unnecessary. Therefore, as a first-order verification of the BBVT's suitability to the task, a largely manual approach is taken in this work, based on the analytical kinematics. This begins with an analysis of the grasping workspace, followed by the creation of detailed waypoints. Collisions are checked using built-in Matlab capabilities, and considerations are made as to how static joint loads can be reduced in critical task poses.

3.1. Grasping Workspace

The standardized grasping interface on the exposed top of each BB segment enforces an ideal vertical grasping pose such that the corresponding BBVT joint configuration has $\theta_t = 0$ and $\theta_t = 6$. Viewed from above, the vertical dimension corresponding to the elevator position d_1 collapses. The remaining joint variables θ_2, d_3, θ_4 and θ_5 and their limits define a planar workspace that constrains the reachable grasps and within which every point is reachable with arbitrary gripper orientation about the vertical axis. Figure 4 depicts this planar workspace overlaid on the BB segments as seen from the upper port, confirming their reachability with the current BBVT design and BB segment grasping interface layout, though the two outboard lateral segments are critically close to the workspace boundary. Figure 4 also displays the x–y location of each BB segment's center of mass, confirming the off-center grasping locations that precipitate large moments for the BBVT to overcome during preloading and manipulation.

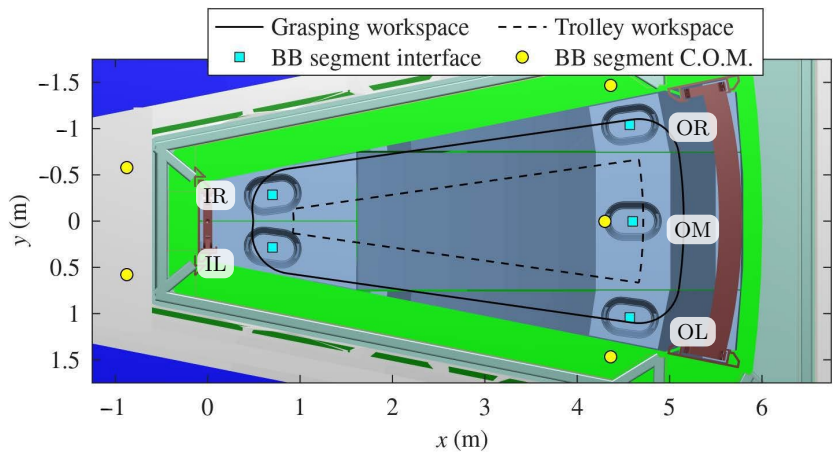

Figure 4. Grasping workspace of the BB vertical transporter within the upper port, viewed from above. BB segments are labeled according to their shorthand names, OM: outboard middle, OR: outboard right, OL: outboard left, IR: inboard right, and IL: inboard left.

3.2. Waypoints

A first step towards detailed motion planning for the BB segment replacement tasks is to choose collision-free waypoints that can generate collision-free trajectories when interpolated by polynomials or other functions in joint space. This is done by first using the available CAD models to position the BB segments within the vacuum vessel, upper port, and cask. Then, the inverse kinematic solution procedures in Section 2.2 can be used to calculate joint-space waypoints based on these desired BB segment (and hence end-effector) poses.

Special attention must be paid to the grasping and preloading pose T_i dictated by the grasping interface of the target BB segment, as well as the final pose T_c with the BBVT holding the segment in the cask. The former partially determines the peak static joints loads, while the latter can be chosen to minimize medium-term holding loads and balance the BB segment center of mass inside the cask to reduce dynamic loads on the cask transport system.

3.2.1. BB Segment Grasping Pose

As can be seen in Figure 5a, the standardized BB segment interface has a major and minor axis. The BB segment frame $\{I\}$ is centered on the interface, with x_I along the major axis and y_I along the minor such that $\{I\}$ and the BBVT gripper TCP frame $\{G\}$ are coincident and aligned when the segment is grasped. For the mounted BB segment, the interface major axis forms an angle ϕ with the global x-axis. This interface angle ϕ influences the BBVT joint loads during segment preloading and manipulation. For simplicity, preloading requires that the axes of the BBVT's two "tilting" joints (θ_t and θ_6) be perpendicular. The θ_6-axis is mechanically constrained to be parallel with the minor axis of the interface, so the θ_t-axis must be parallel with the interface major axis for preloading. It can be shown that the angle that the axis of θ_t makes with the global x-axis is precisely θ_2, so $\theta_2 = \phi$ and thus ϕ, once chosen, must adhere to the joint limits of θ_2 ($\pm 8.12°$). The constraint on θ_2 then leads to there being only two IK solutions for the grasping and preloading pose T_I once ϕ is known together with the interface location. In practice, one IK solution is outside the reachable workspace, so the joint configuration is fully determined for every BB segment.

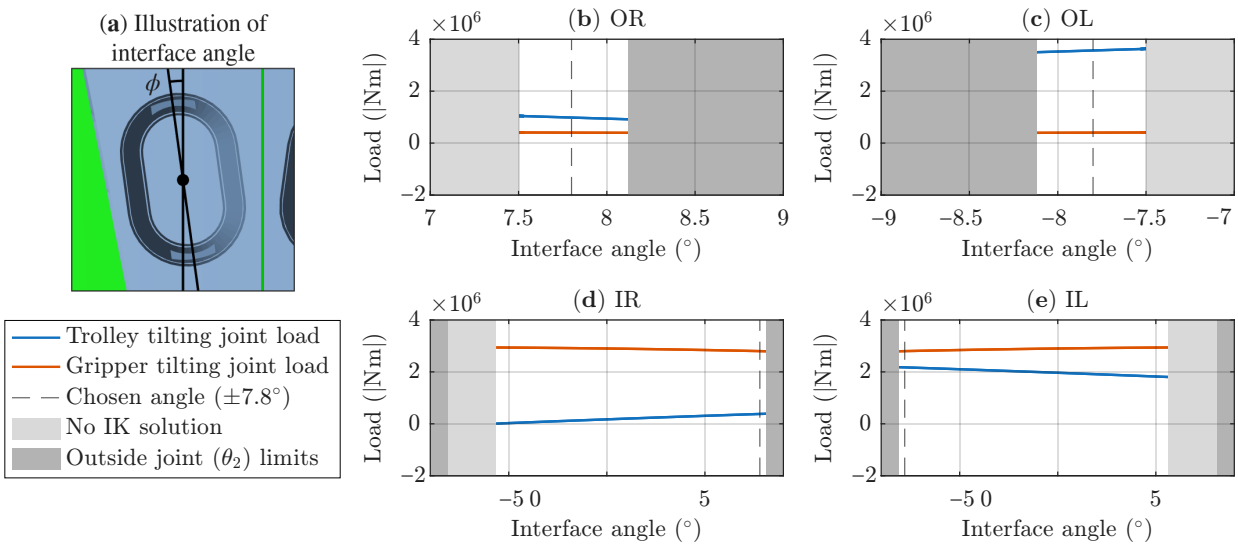

Figure 5. Loads on the trolley tilting and gripper tilting joints when holding each of the lateral BB segments in the initial position, as a function of the interface angle ϕ.

The inverse kinematics solution from Section 2.3 together with Equation (53) are used to calculate the joint loads for different choices of ϕ; these are shown in Figure 5b–e. Only a narrow range of ϕ are acceptable for the outboard segments. Also, for both inboard and outboard segments, the dominant tilting joint load is minimized by choosing ϕ close to the joint limits. Thus, a reasonable choice is to use a unified value of $\phi = \pm 7.8°$ for all the BB segments, as this is near to the middle of the narrow range of acceptable values for the outboard segments, and nearly minimizes the gripper tilting joint load when preloading the inboard segments.

3.2.2. Pose with BB Segment in Cask

The BB segment must be held securely inside the cask over a medium timeframe as the cask is transported to the active maintenance facility. Static joint loads should be minimized for this pose T_c. In addition, the BB segment's center of mass should be centered in the cask to increase stability and reduce dynamic moments affecting the cask transport system.

The static moment on the gripper tilting joint can be minimized by choosing a joint angle θ_6 that minimizes the horizontal distance from the held BB segment center of mass to frame $\{6\}$. If ${}^6x_c$ and ${}^6y_c$ are the x and y coordinates in frame $\{6\}$ of the BB segment center of mass when holding the segment, then the optimal holding angle is $\theta_6 = \arctan\left({}^6x_c / {}^6y_c\right)$. This gives $-2.92°$ for the outboard middle segment, $-1.45°$ for the outboard lateral segments, and $-12.49°$ for the inboard segments. As the inboard segments' optimal holding angle exceeds the joint limits, $\theta_6 = -8°$ is used.

The cask profile is trapezoidal, with the x and y coordinates of the geometric centroid relative to the base frame given by:

$$C = \left(\frac{(2a+b)(2h_c)}{3(a+b)} - x_h,\ 0 \right) \tag{54}$$

where $a = 1.4\,\text{m}$, $b = 4.5\,\text{m}$, $h_c = 7.1\,\text{m}$, and $x_h = 0.555\,\text{m}$. Thus, the position of T_c is constrained.

3.2.3. Intermediate Poses, Summary and Duration Estimate

The remaining poses are defined based on fulfilling the manipulation of the BB segment to or from the cask while avoiding collisions in the limited space within the vacuum vessel and upper port based on preliminary CAD geometry for a DEMO tokamak. The ordered list of chosen gripper TCP poses for the removal of each BB segment is summarized in Table 4 using transformation matrices. The removal order is outboard middle, outboard left, outboard right, inboard right, and inboard left. The resulting joint-space waypoints after solving the inverse kinematics of the outboard and inboard right segments are summarized in Figure 6. Finally, the 10 waypoints for removal of the outboard right BB segment are visualized in Figure 7. All waypoints have been checked for collision between the held BB segment and the upper port and cask using Matlab Robotics System Toolbox's voxelized hierarchical approximate convex decomposition (VHACD) collision solver together with a URDF model of the BBVT, BB, and environment.

The BBVT has been designed to move slowly for safety. A very rough estimate of the time required for BB handling can be made based on the number of waypoints, assuming the average duration of each trajectory part between waypoints is 10 min. Then, the total BB handling time required for the removal and replacement of blankets from all 16 tokamak sectors is on the order of $(2)(16)(10\,\text{min})(8+9+9+7+6)/(1440\,\text{min/day}) \approx 9$ days.

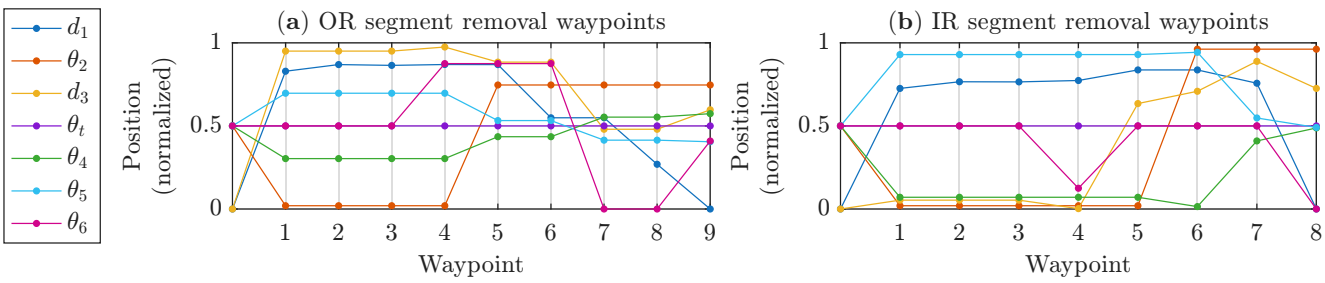

Figure 6. Joint-space waypoints for outboard and inboard right BB segment removal. Joint positions have been normalized with respect to their limits; see Table 1.

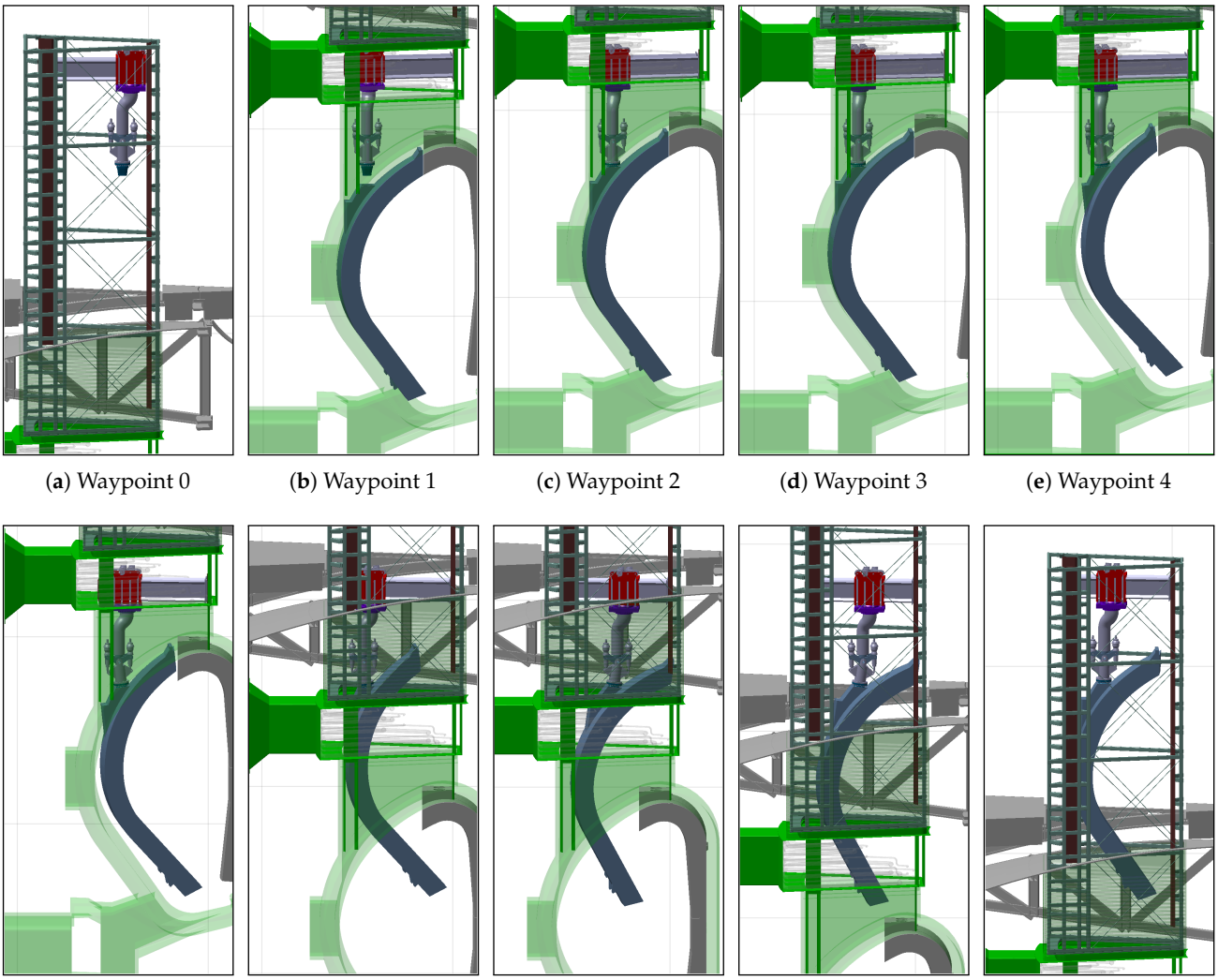

(**a**) Waypoint 0 (**b**) Waypoint 1 (**c**) Waypoint 2 (**d**) Waypoint 3 (**e**) Waypoint 4

(**f**) Waypoint 5 (**g**) Waypoint 6 (**h**) Waypoint 7 (**i**) Waypoint 8 (**j**) Waypoint 9

Figure 7. Visualization of the handling waypoints for the outboard right BB segment.

Table 4. The handling waypoint poses of each BB segment. Each is a homogeneous transformation matrix $\boldsymbol{T}_{wpi}$ defining the gripper TCP pose relative to the global frame. The poses are calculated with reference to known poses $\boldsymbol{T}_{home}$, $\boldsymbol{T}_i$ (the ungrasped BB segment interface), and $\boldsymbol{T}_c$ (the holding pose in the cask) and previous waypoint poses. $\boldsymbol{T}_P(x, y, z)$ are transformation matrices from translations (in meters), and $\boldsymbol{T}_R(\theta_z, \theta_y, \theta_x)$ from Euler angles (in degrees). Post-multiplication modifies the pose in the local frame while pre-multiplication modifies the pose in the global frame.

	Waypoint	Middle BB Segment	Left BB Segments	Right BB Segments
Outboard BB segments	$\boldsymbol{T}_{wp0}$	$\boldsymbol{T}_{home}$	$\boldsymbol{T}_{home}$	$\boldsymbol{T}_{home}$
	$\boldsymbol{T}_{wp1}$	$\boldsymbol{T}_P(0,0,-1)\boldsymbol{T}_{i,OM}$	$\boldsymbol{T}_P(0,0,-1)\boldsymbol{T}_{i,OL}$	$\boldsymbol{T}_P(0,0,-1)\boldsymbol{T}_{i,OR}$
	$\boldsymbol{T}_{wp2}$	$\boldsymbol{T}_{i,OM}$	$\boldsymbol{T}_{i,OL}$	$\boldsymbol{T}_{i,OR}$
	$\boldsymbol{T}_{wp3}$	$\boldsymbol{T}_P(0,0,-0.12)\boldsymbol{T}_{wp2}$	$\boldsymbol{T}_P(0,0,-0.12)\boldsymbol{T}_{wp2}$	$\boldsymbol{T}_P(0,0,-0.12)\boldsymbol{T}_{wp2}$
	$\boldsymbol{T}_{wp4}$	$\boldsymbol{T}_{wp3}\boldsymbol{T}_P(-0.1,0,0.12)\boldsymbol{T}_R(0,-6,0)$	$\boldsymbol{T}_{wp3}\boldsymbol{T}_P(-0.1,0,0.12)\boldsymbol{T}_R(0,-6,0)$	$\boldsymbol{T}_{wp3}\boldsymbol{T}_P(-0.1,0,0.12)\boldsymbol{T}_R(0,-6,0)$
	$\boldsymbol{T}_{wp5}$	$\boldsymbol{T}_P(0,0,-8)\boldsymbol{T}_{wp4}$	$\boldsymbol{T}_{wp4}\boldsymbol{T}_P(-0.15,-1.2,0)$	$\boldsymbol{T}_{wp4}\boldsymbol{T}_P(-0.15,1.2,0)$
	$\boldsymbol{T}_{wp6}$	$\boldsymbol{T}_P(-1,0,0)\boldsymbol{T}_{wp5}\boldsymbol{T}_R(0,14,0)$	$\boldsymbol{T}_P(0,0,-8)\boldsymbol{T}_{wp5}$	$\boldsymbol{T}_P(0,0,-8)\boldsymbol{T}_{wp5}$
	$\boldsymbol{T}_{wp7}$	$\boldsymbol{T}_P(0,0,-7)\boldsymbol{T}_{wp6}$	$\boldsymbol{T}_{wp6}\boldsymbol{T}_R(0,6,0)\boldsymbol{T}_P(-1.1,0,0)\boldsymbol{T}_R(0,8,0)$	$\boldsymbol{T}_{wp6}\boldsymbol{T}_R(0,6,0)\boldsymbol{T}_P(-1.1,0,0)\boldsymbol{T}_R(0,8,0)$
	$\boldsymbol{T}_{wp8}$	$\boldsymbol{T}_{c,OM}$	$\boldsymbol{T}_P(0,0,-7)\boldsymbol{T}_{wp7}$	$\boldsymbol{T}_P(0,0,-7)\boldsymbol{T}_{wp7}$
	$\boldsymbol{T}_{wp9}$	–	$\boldsymbol{T}_{c,OL}$	$\boldsymbol{T}_{c,OR}$

Table 4. *Cont.*

	Waypoint	Middle BB Segment	Left BB Segments	Right BB Segments
Inboard BB segments	$\boldsymbol{T}_{wp0}$		$\boldsymbol{T}_{home}$	$\boldsymbol{T}_{home}$
	$\boldsymbol{T}_{wp1}$		$\boldsymbol{T}_P(0,0,-1)\boldsymbol{T}_{i,IL}$	$\boldsymbol{T}_P(0,0,-1)\boldsymbol{T}_{i,IR}$
	$\boldsymbol{T}_{wp2}$		$\boldsymbol{T}_{i,IL}$	$\boldsymbol{T}_{i,IR}$
	$\boldsymbol{T}_{wp3}$		$\boldsymbol{T}_P(0,0,-0.02)\boldsymbol{T}_{wp2}$	$\boldsymbol{T}_P(0,0,-0.02)\boldsymbol{T}_{wp2}$
	$\boldsymbol{T}_{wp4}$	*(No such BB segment)*	$\boldsymbol{T}_{wp3}\boldsymbol{T}_P(0,0,0.2)\boldsymbol{T}_R(0,6,0)$	$\boldsymbol{T}_{wp3}\boldsymbol{T}_P(0,0,0.2)\boldsymbol{T}_R(0,6,0)$
	$\boldsymbol{T}_{wp5}$		$\boldsymbol{T}_{wp4}\boldsymbol{T}_R(0,-6,0)\boldsymbol{T}_P(2.2,0,1.8)$	$\boldsymbol{T}_{wp4}\boldsymbol{T}_R(0,-6,0)\boldsymbol{T}_P(2.2,0,1.6)$
	$\boldsymbol{T}_{wp6}$		$\boldsymbol{T}_P(0,-0.8,0)\boldsymbol{T}_{wp5}$	$\boldsymbol{T}_P(0.27,0.96,0)\boldsymbol{T}_{wp5}$
	$\boldsymbol{T}_{wp7}$		$\boldsymbol{T}_{c,IL}$	$\boldsymbol{T}_P(1.5,0,-2)\boldsymbol{T}_{wp6}$
	$\boldsymbol{T}_{wp8}$		–	$\boldsymbol{T}_{c,IR}$

3.3. Static Loads

The static loads at the BBVT joints have been calculated for each of the waypoints. Due to the design of the BBVT, the joint 2 and 3 actuators do not experience any direct static loads. Joints 4 and 5 likewise do not experience any static loads when $\theta_t = 0$, as assumed in the simplified case. As the elevator is modeled as a single vertical prismatic joint, the static load it experiences (the total load on all the chains) is simply the BB segment weight regardless of the BBVT configuration.

Thus, only the two tilting joints experience varying static loads based on the BBVT configuration at each waypoint. These are shown in Figure 8. The results indicate that the initial lifting (waypoint 2 for all segments) generally represents the worst load case, especially for the trolley tilting joint.

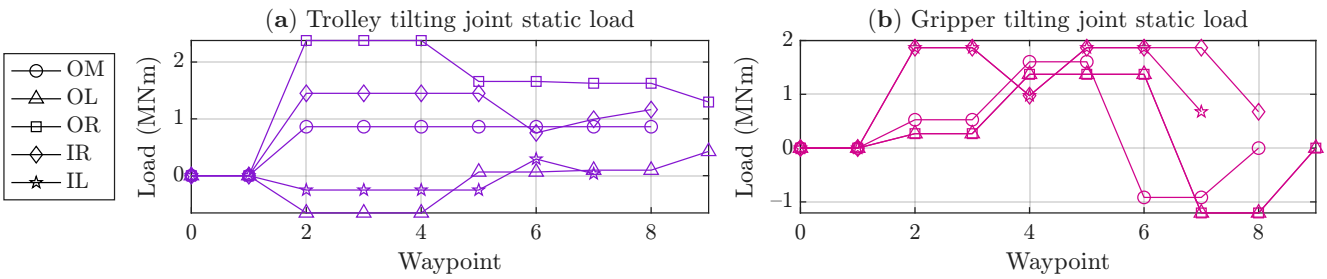

Figure 8. Configuration -dependent static load on each tilting joint for all waypoints and BB segments.

4. Conclusions

Vertical breeding blanket maintenance in a DEMO-type tokamak power plant requires the careful design and application of a heavy-duty and dexterous robotic remote handling tool such as the 7-jointed BBVT. Accurate and precise control are required at every stage of the BB maintenance task to avoid collisions and ensure safety despite mechanical and environmental disturbances. The redundant nature of the BBVT mechanism allows operational flexibility due to the availability of infinite inverse kinematic solutions, yet redundancy resolution is challenging in itself. Numerical inverse kinematics algorithms are generally used that can iteratively approximate a single solution while optimizing and satisfying additional criteria and constraints. On the other hand, analytical solutions are more accurate, tend to be faster, and bypass classic numerical weaknesses such as ill-conditioning of the constraint Jacobian near kinematic singularities.

In this work, an analytical kinematic model of the BBVT was formulated and verified by comparison to numerical results from MSC Adams. Based on the model, the inverse kinematic problem was solved analytically for cases relevant to the BB handling task, in which the position of the trolley tilting joint is expected to always be fixed or prescribed. Two kinematically distinct scenarios were thus analyzed: when the trolley tilting joint variable θ_t is non-zero and when it is zero. In the former case, the BBVT loses its redundant

character and the number of IK solutions becomes four or less. In the latter case, redundancy is maintained but the range of IK solutions can be parameterized in terms of the trolley's angular position on a circle in space. Although numerical algorithms remain necessary if θ_t is free and unknown, the developed analytical IK algorithm for $\theta_t \neq 0$ was found to be 53× faster than the next-fastest numerical IK algorithm in Matlab (`BFGS`) while the algorithm for $\theta_t = 0$ was 84 × faster. In both cases, the analytical algorithms provided several precise solutions rather than one approximation.

As part of the kinematic analysis, the geometric Jacobian was also obtained in forms for when θ_t is unknown, fixed, and zero, allowing for the convenient calculation of configuration-dependent static joint loads. Indeed, this work next applied the IK algorithms and Jacobian to create detailed collision-free waypoints achieving the BB segment removal tasks while minimizing static loads for the crucial grasping and cask-holding poses. The lack of collisions was checked using VHACD in Matlab. Finally, a first approximation of the total BB handling time for the maintenance task was calculated as 9 days.

The kinematic model, high-performance analytical inverse kinematic algorithms, and statics-based motion planning presented in this work support the feasibility of the BBVT for the BB maintenance task and create a strong foundation for future work. The proposed waypoints can be used for complete trajectory generation, while the kinematic model forms a basis for future dynamic modelling and model-based real-time control development. The kinematic modelling must also be extended to cover the complex joint sub-mechanisms and structures, and sources of flexibility and backlash should be investigated to enable modelling and verifying the preloading process in detail. Finally, work is ongoing to further validate models and results with physical prototypes.

Author Contributions: Conceptualization, C.B., R.M. and G.J.; methodology, H.D.; software, H.D.; validation, H.D.; formal analysis, H.D.; investigation, H.D.; resources, X.Z.; data curation, H.D.; writing—original draft preparation, H.D.; writing—review and editing, X.Z.; visualization, H.D.; supervision, X.Z.; project administration, X.Z.; and funding acquisition, X.Z. All authors have read and agreed to the published version of the manuscript.

Funding: This work has been carried out within the framework of the EUROfusion Consortium, funded by the European Union via the Euratom Research and Training Programme (Grant Agreement No. 101052200—EUROfusion).

Data Availability Statement: The dataset is available on request from the authors.

Conflicts of Interest: The authors declare no conflicts of interest. The funders had no role in the design of the study; in the collection, analyses, or interpretation of data; in the writing of the manuscript; or in the decision to publish the results.

Appendix A. Velocity Propagation and Jacobian

The instantaneous rigid propagation of the three-element angular and linear velocity vectors $\boldsymbol{\omega}$ and $\boldsymbol{v}$ from link i to link $i+1$ can be stated as:

$$\boldsymbol{\omega}_{i+1} = {}^{i+1}_{i}\boldsymbol{R}\boldsymbol{\omega}_i + \begin{bmatrix} \mathbf{0} \\ \mathbf{0} \\ \dot{\theta}_{i+1} \end{bmatrix} \tag{A1}$$

$$\boldsymbol{v}_{i+1} = {}^{i+1}_{i}\boldsymbol{R}\left(\boldsymbol{v}_i + \boldsymbol{\omega}_i \times {}^{i}\boldsymbol{P}_{i+1}\right) \tag{A2}$$

when the two links are connected by a revolute joint, or as

$$\boldsymbol{\omega}_{i+1} = {}^{i+1}_{i}\boldsymbol{R}\boldsymbol{\omega}_i \tag{A3}$$

$$\boldsymbol{v}_{i+1} = {}^{i+1}_{i}\boldsymbol{R}\left(\boldsymbol{v}_i + \boldsymbol{\omega}_i \times {}^{i}\boldsymbol{P}_{i+1}\right) + \begin{bmatrix} 0 \\ 0 \\ \dot{d}_{i+1} \end{bmatrix} \tag{A4}$$

when the two links are connected by a prismatic joint [25]. Here, R is a 3×3 rlegendsotation matrix defining the relative link frame orientation and P is a three-element vector defining the relative link frame position. The resulting velocity of each link is expressed relative to its own frame. By applying these equations iteratively outwards from the first link ($i = 1$) to the final link while assuming a stationary global frame (a.k.a. base link, $i = 0$), the angular and linear velocities of the end effector relative to the outermost frame link ($i = 6$ for the BBVT) can be found. The resulting six equations can be stated in matrix form:

$$\begin{bmatrix} \boldsymbol{v}_6 \\ \boldsymbol{\omega}_6 \end{bmatrix} = {}^{6}\boldsymbol{J}_6 \begin{bmatrix} \dot{d}_1 & \dot{\theta}_2 & \dot{d}_3 & \dot{\theta}_t & \dot{\theta}_4 & \dot{\theta}_5 & \dot{\theta}_6 \end{bmatrix}^{\top} = {}^{6}\boldsymbol{J}_6 \dot{\boldsymbol{\Theta}}, \tag{A5}$$

where ${}^{6}\boldsymbol{J}_6$ is the 6×7 Jacobian matrix expressed relative to the frame of link 6. It is too unwieldy to write directly in its analytical form. However, it happens that the equations for the end effector velocity, and thereby the Jacobian, simplify significantly when expressed relative to the frame of link 5 instead of link 6, as the dependence on θ_6 vanishes. The rotation of the velocity equations and Jacobian can be achieved as so:

$$\begin{bmatrix} {}^{5}_{6}\boldsymbol{R} & 0 \\ 0 & {}^{5}_{6}\boldsymbol{R} \end{bmatrix} \begin{bmatrix} \boldsymbol{v}_6 \\ \boldsymbol{\omega}_6 \end{bmatrix} = \begin{bmatrix} {}^{5}_{6}\boldsymbol{R} & 0 \\ 0 & {}^{5}_{6}\boldsymbol{R} \end{bmatrix} {}^{6}\boldsymbol{J}_6 \dot{\boldsymbol{\Theta}} \tag{A6}$$

$$\begin{bmatrix} {}^{5}\boldsymbol{v}_6 \\ {}^{5}\boldsymbol{\omega}_6 \end{bmatrix} = {}^{5}\boldsymbol{J}_6 \dot{\boldsymbol{\Theta}}, \tag{A7}$$

where the rotation matrix ${}^{5}_{6}\boldsymbol{R}$ has the following form according to the kinematic model established by the D-H parameters:

$${}^{5}_{6}\boldsymbol{R} = {}^{6}_{5}\boldsymbol{R}^{\top} = \begin{bmatrix} \mathrm{c}_6 & -\mathrm{s}\,6 & 0 \\ 0 & 0 & -1 \\ \mathrm{s}\,6 & \mathrm{c}_6 & 0 \end{bmatrix} \tag{A8}$$

The Jacobian matrix ${}^{5}\boldsymbol{J}_6$ of Equation (A7) can then be written as:

$${}^{5}\boldsymbol{J}_6 = \begin{bmatrix} \mathrm{s}_{45}\,\mathrm{s}_t & k\,\mathrm{s}_5\,\mathrm{c}_t + l\,\mathrm{c}_{45}\,\mathrm{s}_t + d_3\,\mathrm{s}_{45}\,\mathrm{c}_t - h\,\mathrm{c}_{45}(1-\mathrm{c}_t) & \mathrm{c}_{45} & -l\,\mathrm{s}_{45} & k\,\mathrm{s}_5 & 0 & 0 \\ \mathrm{c}_{45}\,\mathrm{s}_t & k\,\mathrm{c}_5\,\mathrm{c}_t - l\,\mathrm{s}_{45}\,\mathrm{s}_t + d_3\,\mathrm{c}_{45}\,\mathrm{c}_t + h\,\mathrm{s}_{45}(1-\mathrm{c}_t) & -\mathrm{s}_{45} & -l\,\mathrm{c}_{45} & k\,\mathrm{c}_5 & 0 & 0 \\ \mathrm{c}_t & -\mathrm{s}_t\,(d_3 + k\,\mathrm{c}_4) & 0 & k\,\mathrm{s}_4 - h & 0 & 0 & 0 \\ 0 & \mathrm{s}_{45}\,\mathrm{s}_t & 0 & \mathrm{c}_{45} & 0 & 0 & 0 \\ 0 & \mathrm{c}_{45}\,\mathrm{s}_t & 0 & -\mathrm{s}_{45} & 0 & 0 & -1 \\ 0 & \mathrm{c}_t & 0 & 0 & 1 & 1 & 0 \end{bmatrix}, \tag{A9}$$

in which the fourth column should be removed if the trolley tilting joint is considered passive and immobile, obtaining a full-rank, square matrix.

References

1. Federici, G.; Baylard, C.; Beaumont, A.; Holden, J. The Plan Forward for EU DEMO. *Fusion Eng. Des.* **2021**, *173*, 112960. [CrossRef]
2. Federici, G. Testing Needs for the Development and Qualification of a Breeding Blanket for DEMO. *Nucl. Fusion* **2023**, *63*, 125002. [CrossRef]
3. Buckingham, R.; Loving, A. Remote-Handling Challenges in Fusion Research and Beyond. *Nature Phys.* **2016**, *12*, 391–393. [CrossRef]
4. Rolfe, A.C. A Perspective on Fusion Relevant Remote Handling Techniques. *Fusion Eng. Des.* **2007**, *82*, 1917–1923. [CrossRef]

5. Ribeiro, I.; Damiani, C.; Tesini, A.; Kakudate, S.; Siuko, M.; Neri, C. The Remote Handling Systems for ITER. *Fusion Eng. Des.* **2011**, *86*, 471–477. [CrossRef]
6. Magnani, E.; Cachon, L.; Ihli, T.; West, J. Recent In-Vessel Integration Concepts for a European DEMO Reactor. *Fusion Sci. Technol.* **2009**, *56*, 935–939. [CrossRef]
7. Loving, A.; Crofts, O.; Sykes, N.; Iglesias, D.; Coleman, M.; Thomas, J.; Harman, J.; Fischer, U.; Sanz, J.; Siuko, M.; et al. Pre-Conceptual Design Assessment of DEMO Remote Maintenance. *Fusion Eng. Des.* **2014**, *89*, 2246–2250. [CrossRef]
8. Coleman, M.; Sykes, N.; Cooper, D.; Iglesias, D.; Bastow, R.; Loving, A.; Harman, J. Concept for a Vertical Maintenance Remote Handling System for Multi Module Blanket Segments in DEMO. *Fusion Eng. Des.* **2014**, *89*, 2347–2351. [CrossRef]
9. Crofts, O.; Loving, A.; Iglesias, D.; Coleman, M.; Siuko, M.; Mittwollen, M.; Queral, V.; Vale, A.; Villedieu, E. Overview of Progress on the European DEMO Remote Maintenance Strategy. *Fusion Eng. Des.* **2016**, *109–111*, 1392–1398. [CrossRef]
10. Tobita, K.; Hiwatari, R.; Utoh, H.; Miyoshi, Y.; Asakura, N.; Sakamoto, Y.; Someya, Y.; Homma, Y.; Nakamura, M.; Hoshino, K.; et al. Overview of the DEMO Conceptual Design Activity in Japan. *Fusion Eng. Des.* **2018**, *136*, 1024–1031. [CrossRef]
11. Kwon, S.; Im, K.; Hong, S.H.; Lee, H.; Rognlien, T.D.; Meyer, W.; Kim, K. Recent Progress in the Design of the K-DEMO Divertor. *Fusion Eng. Des.* **2020**, *159*, 111770. [CrossRef]
12. Zhao, W.; Shi, S.; Cheng, Y.; Huang, J.; Sun, H.; Pan, H.; Yang, S.; Zhang, Y. Strategy Study and Preliminary Conceptual Design of the Remote Maintenance Systems for in Vessel Components of CFETR. *J. Fusion Energy* **2020**, *39*, 67–76. [CrossRef]
13. Kim, S.; Jung, S.H.; Kim, C.H. Preventive Maintenance and Remote Inspection of Nuclear Power Plants Using Tele-Robotics. In Proceedings of the 1999 IEEE/RSJ International Conference on Intelligent Robots and Systems. Human and Environment Friendly Robots with High Intelligence and Emotional Quotients (Cat. No.99CH36289), Kyongju, Republic of Korea, 17–21 October 1999; Volume 1, pp. 603–608. [CrossRef]
14. Bogue, R. Robots in the Nuclear Industry: A Review of Technologies and Applications. *Ind. Robot.* **2011**, *38*, 113–118. [CrossRef]
15. Tochilin, A.V.; Voronkov, I.E.; Alabin, A.V. Experience and Prospects of Using Robotics in the Nuclear Power Industry. *IOP Conf. Ser. Mater. Sci. Eng.* **2021**, *1047*, 012193. [CrossRef]
16. Guzman, R.; Navarro, R.; Ferre, J.; Moreno, M. RESCUER: Development of a Modular Chemical, Biological, Radiological, and Nuclear Robot for Intervention, Sampling, and Situation Awareness. *J. Field Robot.* **2016**, *33*, 931–945. [CrossRef]
17. Zhonglin, Z.; Bin, F.; Liquan, L.; Encheng, Y. Design and Function Realization of Nuclear Power Inspection Robot System. *Robotica* **2021**, *39*, 165–180. [CrossRef]
18. Skilton, R.; Hamilton, N.; Howell, R.; Lamb, C.; Rodriguez, J. MASCOT 6: Achieving High Dexterity Tele-Manipulation with a Modern Architectural Design for Fusion Remote Maintenance. *Fusion Eng. Des.* **2018**, *136*, 575–578. [CrossRef]
19. Bachmann, C.; Gliss, C.; Janeschitz, G.; Steinbacher, T.; Mozzillo, R. Conceptual Study of the Remote Maintenance of the DEMO Breeding Blanket. *Fusion Eng. Des.* **2022**, *177*, 113077. [CrossRef]
20. Bachmann, C.; Janeschitz, G.; Fanelli, P.; Gliss, C.; Mollicone, P.; Muscat, M.; Stefanini, C.; Steinbacher, T.; Domínguez, J.V.; Vigano, F.; et al. Progress in the Development of the In-Vessel Transporter and the Upper Port Cask for the Remote Replacement of the DEMO Breeding Blanket. *Fusion Eng. Des.* **2023**, *194*, 113715. [CrossRef]
21. Steinbacher, T.; Bachmann, C.; Gliss, C.; Janeschitz, G.; Mozzillo, R. Design of the Gripper Interlock That Engages with the DEMO Breeding Blanket during Remote Maintenance. *Fusion Eng. Des.* **2023**, *193*, 113641. [CrossRef]
22. Vizvary, Z.; Richiusa, M.L.; Bachmann, C.; Maione, I.A.; Vorpahl, C. Status of the DEMO Blanket Attachment System and Remaining Challenges. *Fusion Eng. Des.* **2020**, *151*, 111357. [CrossRef]
23. Lakshmi Narayanan, V.; Narayan, J.; Gritli, H.; Dwivedy, S.K. A Decade of Inverse Kinematics Methods for Serial Manipulators: A Systematic Review. *J. Field Robot.* **2026**, *43*, 184–229. [CrossRef]
24. Frosi, P.; Bachmann, C.; Cismondi, F. EU-DEMO Breeding Blanket Temperature Evaluation before Remote Maintenance Operation. *Fusion Eng. Des.* **2019**, *146*, 2561–2566. [CrossRef]
25. Craig, J.J. *Introduction to Robotics: Mechanics and Control*, 3rd ed.; Pearson Prentice Hall: Hoboken, NJ, USA, 2005.
26. Bachmann, C.; Gliss, C.; H′artl, T.; Hernandez, F.; Maione, I.; Steinbacher, T.; Vizvary, Z. Mechanical Support Concept of the DEMO Breeding Blanket. *Fusion Eng. Des.* **2021**, *173*, 112840. [CrossRef]
27. Durocher, H.; Bachmann, C.; Mozzillo, R.; Janeschitz, G.; Zhang, X. A Spatial Five-Bar Linkage as a Tilting Joint of the Breeding Blanket Transporter for the Remote Maintenance of EU DEMO. *Machines* **2025**, *13*, 371. [CrossRef]
28. Whitney, D.E. Resolved Motion Rate Control of Manipulators and Human Prostheses. *IEEE Trans. Man-Mach. Syst.* **1969**, *10*, 47–53. [CrossRef]
29. Colomé, A.; Torras, C. Closed-Loop Inverse Kinematics for Redundant Robots: Comparative Assessment and Two Enhancements. *IEEE/ASME Trans. Mechatron.* **2015**, *20*, 944–955. [CrossRef]
30. Chan, T.; Dubey, R. A Weighted Least-Norm Solution Based Scheme for Avoiding Joint Limits for Redundant Manipulators. In Proceedings of the [1993] Proceedings IEEE International Conference on Robotics and Automation, Atlanta, GA, USA, 2–6 May 1993; Volume 3, pp. 395–402. [CrossRef]

31. Automatic Supervisory Control of the Configuration and Behavior of Multibody Mechanisms. *IEEE Trans. Syst. Man, Cybern.* **1977**, *7*, 868–871. [CrossRef]
32. Egeland, O. Task-Space Tracking with Redundant Manipulators. *IEEE J. Robot. Autom.* **1987**, *3*, 471–475. [CrossRef]
33. Hoang, P.T.; Choi, Y.S.; Rhee, I.; Kang, G.; Choi, H.R. A New Torque Minimization Method for Heavy-Duty Redundant Manipulators Used in Nuclear Decommissioning Tasks. *Intell. Serv. Robot.* **2021**, *14*, 459–469. [CrossRef]
34. Hassan, A.A.; El-Habrouk, M.; Deghedie, S. Inverse Kinematics of Redundant Manipulators Formulated as Quadratic Programming Optimization Problem Solved Using Recurrent Neural Networks: A Review. *Robotica* **2020**, *38*, 1495–1512. [CrossRef]
35. Shimizu, M.; Kakuya, H.; Yoon, W.K.; Kitagaki, K.; Kosuge, K. Analytical Inverse Kinematic Computation for 7-DOF Redundant Manipulators With Joint Limits and Its Application to Redundancy Resolution. *IEEE Trans. Robot.* **2008**, *24*, 1131–1142. [CrossRef]
36. Singh, g.; Claassens, J. An Analytical Solution for the Inverse Kinematics of a Redundant 7DoF Manipulator with Link Offsets. In Proceedings of the 2010 IEEE/RSJ International Conference on Intelligent Robots and Systems, Taipei, Taiwan, 18–22 October 2010; p. 2982. [CrossRef]
37. Shi, X.; Guo, Y.; Chen, X.; Chen, Z.; Yang, Z. Kinematics and Singularity Analysis of a 7-DOF Redundant Manipulator. *Sensors* **2021**, *21*, 7257. [CrossRef]
38. Goldfarb, D. Extension of Davidon's Variable Metric Method to Maximization Under Linear Inequality and Equality Constraints. *SIAM J. Appl. Math.* **1969**, *17*, 739–764. [CrossRef]
39. Sugihara, T. Solvability-Unconcerned Inverse Kinematics by the Levenberg–Marquardt Method. *IEEE Trans. Robot.* **2011**, *27*, 984–991. [CrossRef]
40. Badreddine, H.; Vandewalle, S.; Meyers, J. Sequential Quadratic Programming (SQP) for Optimal Control in Direct Numerical Simulation of Turbulent Flow. *J. Comput. Phys.* **2014**, *256*, 1–16. [CrossRef]
41. Kingston, Z.; Moll, M.; Kavraki, L.E. Sampling-Based Methods for Motion Planning with Constraints. *Annu. Rev. Control Robot. Auton. Syst.* **2018**, *1*, 159–185. [CrossRef]
42. Yang, L.; Qi, J.; Song, D.; Xiao, J.; Han, J.; Xia, Y. Survey of Robot 3D Path Planning Algorithms. *J. Control. Sci. Eng.* **2016**, *2016*, 7426913. [CrossRef]
43. Tamizi, M.G.; Yaghoubi, M.; Najjaran, H. A Review of Recent Trend in Motion Planning of Industrial Robots. *Int. J. Intell. Robot. Appl.* **2023**, *7*, 253–274. [CrossRef]
44. Garrett, C.R.; Chitnis, R.; Holladay, R.; Kim, B.; Silver, T.; Kaelbling, L.P.; Lozano-Pérez, T. Integrated Task and Motion Planning. *Annu. Rev. Control Robot. Auton. Syst.* **2021**, *4*, 265–293. [CrossRef]
45. Yang, Z.; Garrett, C.; Fox, D.; Lozano-Pérez, T.; Kaelbling, L.P. Guiding Long-Horizon Task and Motion Planning with Vision Language Models. In Proceedings of the 2025 IEEE International Conference on Robotics and Automation (ICRA), Atlanta, GA, USA, 19–23 May 2025; pp. 16847–16853. [CrossRef]

Disclaimer/Publisher's Note: The statements, opinions and data contained in all publications are solely those of the individual author(s) and contributor(s) and not of MDPI and/or the editor(s). MDPI and/or the editor(s) disclaim responsibility for any injury to people or property resulting from any ideas, methods, instructions or products referred to in the content.